

Article

# Pt-Au/MO<sub>x</sub>-CeO<sub>2</sub> (M = Mn, Fe, Ti) Catalysts for the Co-Oxidation of CO and H<sub>2</sub> at Room Temperature

Xiaowei Hong <sup>1,†</sup>, Ye Sun <sup>1,†</sup>, Tianle Zhu <sup>1,\*</sup> and Zhiming Liu <sup>2,\*</sup>

<sup>1</sup> School of Space and Environment, Beihang University, Beijing 100191, China; hongxiao86@126.com (X.H.); suny@buaa.edu.cn (Y.S.)

<sup>2</sup> State Key Laboratory of Chemical Resource Engineering, Beijing University of Chemical Technology, Beijing 100029, China

\* Correspondence: zhutl@buaa.edu.cn (T.Z.); liuzm@mail.buct.edu.cn (Z.L.); Tel.: +86-10-8231-4215 (T.Z.); +86-10-6442-7356 (Z.L.)

† These authors contributed equally to this work.

Academic Editor: Nikolaos Dimitratos

Received: 9 January 2017; Accepted: 21 February 2017; Published: 27 February 2017

**Abstract:** A series of nanostructured Pt-Au/MO<sub>x</sub>-CeO<sub>2</sub> (M = Mn, Fe, Ti) catalysts were prepared and their catalytic performance for the co-oxidation of carbon monoxide (CO) and hydrogen (H<sub>2</sub>) were evaluated at room temperature. The results showed that MO<sub>x</sub> promoted the CO oxidation of Pt-Au/CeO<sub>2</sub>, but only the TiO<sub>2</sub> could enhance co-oxidation of CO and H<sub>2</sub> over Pt-Au/CeO<sub>2</sub>. Related characterizations were conducted to clarify the promoting effect of MO<sub>x</sub>. Temperature-programmed reduction of hydrogen (H<sub>2</sub>-TPR) and X-ray photoelectron spectroscopy (XPS) results suggested that MO<sub>x</sub> could improve the charge transfer from Au sites to CeO<sub>2</sub>, resulting in a high concentration of Ce<sup>3+</sup> and cationic Au species which benefits for the CO oxidation. In-situ diffuse reflectance infrared Fourier transform spectroscopy (In-situ DRIFTS) results indicated that TiO<sub>2</sub> could facilitate the oxidation of H<sub>2</sub> over the Pt-Au/TiO<sub>2</sub>-CeO<sub>2</sub> catalyst.

**Keywords:** CO; H<sub>2</sub>; Co-oxidation; Pt-Au/MO<sub>x</sub>-CeO<sub>2</sub>; Room temperature

## 1. Introduction

Both H<sub>2</sub> and CO co-exist in space capsule. H<sub>2</sub> mainly originates from the charge–discharge process of battery and CO is released from processes of human metabolism. H<sub>2</sub> and CO, as the typical inflammable and explosive gaseous contaminants, seriously threaten the safety of human and airtight cabin. In addition, long-term exposure to CO causes adverse effects on human health [1]. Therefore, more and more attention has been paid on the simultaneous removal of CO and H<sub>2</sub>. Catalytic oxidation has been regarded as an effective and green technology to eliminate CO and H<sub>2</sub> [2].

Noble metal catalysts for the oxidation of H<sub>2</sub> and CO have been extensively studied recently [3–8]. Pt catalysts were considered as the most active catalysts for H<sub>2</sub> oxidation at room temperature [9]. Previous studies showed that Pt-Ru/C [10] and Pt-Sn/C [11] electrocatalysts exhibited high catalytic performance for the H<sub>2</sub> oxidation, and metallic Pt species were more active than the oxidized Pt species [12,13]. Au catalysts have been reported to be more active than Pt catalysts for CO oxidation [8,14]. CO could be removed at room temperature over Au/CeO<sub>2</sub> [15], Au/TiO<sub>2</sub> [16], Au/MnO<sub>x</sub> [17], and Au/Fe<sub>2</sub>O<sub>3</sub> [18] catalysts. Moreover, cationic Au species were more active than the metallic Au species [18,19].

In order to remove CO and H<sub>2</sub> in space capsule, developing novel catalysts with excellent activity for the co-oxidation of CO and H<sub>2</sub> is desirable. Recently, a few studies related to the co-oxidation of H<sub>2</sub> and CO have been reported [5,6,20–22]. Zhang et al. [21] reported that Pt-Au/CeO<sub>2</sub> bimetallic catalysts with ordered macro-porous and meso-porous structure showed superior catalytic performance for

CO oxidation but not for H<sub>2</sub> oxidation. Ru-Pt bimetallic core-shell nanoparticle catalyst has been developed by Eichhorn et al. [23], however, it could not afford the simultaneous removal of CO and H<sub>2</sub>. Au-Pd/Fe(OH)<sub>x</sub> catalyst with separate Au active sites and Pd active sites was excellent for the complete co-oxidation of H<sub>2</sub> and CO at low temperature [5], but the gas hourly space velocity (GHSV) (20,000 h<sup>-1</sup>) was relatively low. At high GHSV, the oxidation of H<sub>2</sub> was strongly inhibited by the presence of CO [6]. Therefore, the simultaneous removal of H<sub>2</sub> and CO at room temperature at high GHSV still remains challenging. CeO<sub>2</sub> enhanced the oxidation reactions due to its high oxygen storage capacity and redox property [24]. Corma et al. [15] pointed out that nanocrystalline CeO<sub>2</sub> with Ce<sup>3+</sup> ions could adsorb and activate O<sub>2</sub>, thus enhancing the catalyst reactivity. Ordered CeO<sub>2</sub> support with higher surface area could lead to the better dispersion of active sites and also boost oxygen transfer to active platinum species [25]. For the CO and H<sub>2</sub> oxidation, surface diffusion and spillover enhanced oxidation reaction on Pt/CeO<sub>2</sub> [26–28] and Au/CeO<sub>2</sub> catalysts [8,29]. Therefore, CeO<sub>2</sub> nanospheres with meso-structure were promising supports for Au and Pt catalysts. Fe<sub>2</sub>O<sub>3</sub> [30–32], TiO<sub>2</sub> [33,34] and MnO<sub>2</sub> [35–38] were proven to be excellent promoters because of their high oxygen storage capacity and redox property. In addition, preparation methods showed significant effect on the catalytic performance of catalysts [6]. Reduction treatment improved the catalytic activities of Pt catalysts [12] and urea was an excellent precipitant for Au catalysts [39].

According to the above-mentioned understanding, a series of nanostructured Pt-Au/MO<sub>x</sub>-CeO<sub>2</sub> (M = Mn, Fe, Ti) bimetallic catalysts were prepared by the reduction-deposition precipitation method and their performance for the co-oxidation of CO and H<sub>2</sub> under the GHSV of 500,000 h<sup>-1</sup> at room temperature were evaluated. Physical and chemical properties of the Pt-Au/MO<sub>x</sub>-CeO<sub>2</sub> (M = Mn, Fe, Ti) bimetallic catalysts were characterized. Based on the characterization, the relationship between the structure and the catalytic performance has been elucidated.

## 2. Results and Discussion

### 2.1. Catalytic Activities of the Pt-Au/MO<sub>x</sub>-CeO<sub>2</sub> Catalysts

Figure 1 presents the activities of the Pt-Au/MO<sub>x</sub>-CeO<sub>2</sub> catalysts for the catalytic co-oxidation of CO and H<sub>2</sub>. For Pt-Au/CeO<sub>2</sub> catalyst, conversions of CO and H<sub>2</sub> are 93% and 25%, respectively, and then gradually decrease. It is attributed to the CO accumulation on Au and Pt active sites. CO can be completely removed while the conversion of H<sub>2</sub> is low over Pt-Au/MnO<sub>2</sub>-CeO<sub>2</sub> and Pt-Au/Fe<sub>2</sub>O<sub>3</sub>-CeO<sub>2</sub> catalysts. It is encouraging that 100% conversions of CO and H<sub>2</sub> are obtained at room temperature over Pt-Au/TiO<sub>2</sub>-CeO<sub>2</sub> catalyst. However, the conversion of H<sub>2</sub> decreases over Pt-Au/TiO<sub>2</sub>-CeO<sub>2</sub> catalyst due to H<sub>2</sub>O accumulation on the Pt and Au active sites [7]. The oxidation of CO is suppressed by H<sub>2</sub>O when the H<sub>2</sub>O content is over 200 ppm [40]. The inhibiting effect of H<sub>2</sub>O is due to the competitive adsorption between H<sub>2</sub>O and CO molecules on the surface twofold coordinated oxygen site [41]. On the other hand, a competitive adsorption between H<sub>2</sub>O and O<sub>2</sub> molecules also exists due to the accumulation and occupation of H<sub>2</sub>O on the Pt and Au active sites [7].

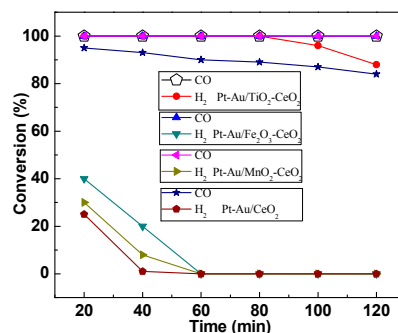


**Figure 1.** The activities of Pt-Au/MO<sub>x</sub>-CeO<sub>2</sub> catalysts for the catalytic co-oxidations of H<sub>2</sub> and CO. Reaction conditions: 100 ppm H<sub>2</sub>/100 ppm CO/room air; temperature: 25 °C; GHSV = 500,000 h<sup>-1</sup>.

## 2.2. Physicochemical Properties of Catalysts

Figure 2 presents the X-ray diffraction (XRD) patterns of the CeO<sub>2</sub> support and Pt-Au/MO<sub>x</sub>-CeO<sub>2</sub> catalysts. All these samples show typical cubic CeO<sub>2</sub> diffraction peaks (JCPDS 43-1002). The diffraction peaks ascribed to MO<sub>x</sub>, Pt and Au species are absent, which indicates that MO<sub>x</sub>, Pt and Au species are highly dispersed on the support. Figure 3 shows the transmission electron microscope (TEM) images of the CeO<sub>2</sub> support and Pt-Au/MO<sub>x</sub>-CeO<sub>2</sub> catalysts. It can be found that CeO<sub>2</sub> support presents nanosphere that is comprised of many small particles with a crystallite size of 5 nm. The contents of Pt and Au species in energy dispersive spectrometer (EDS) results of the Pt-Au/MO<sub>x</sub>-CeO<sub>2</sub> catalysts are close to the theoretical values (1 wt %). Chemical composition and textural properties of Pt-Au/MO<sub>x</sub>-CeO<sub>2</sub> catalysts are seen in Table 1. Compared with the X-ray photoelectron spectroscopy (XPS) results presented in Table 1, contents of Pt and Au species in EDS results are higher, indicating that parts of Pt and Au species are distributed on the surface of the CeO<sub>2</sub> nanoparticles. Brunauer–Emmett–Teller (BET) surface areas of Pt-Au/MO<sub>x</sub>-CeO<sub>2</sub> catalysts decrease due to the introduction of MO<sub>x</sub>. The dispersions of metal on Pt-Au/MO<sub>x</sub>-CeO<sub>2</sub> catalysts are very close due to the same preparation method.

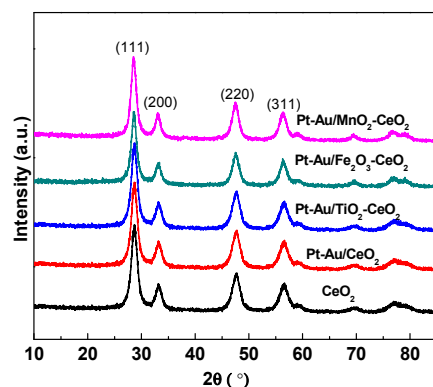


Figure 2. XRD patterns of CeO<sub>2</sub> support and Pt-Au/MO<sub>x</sub>-CeO<sub>2</sub> catalysts.

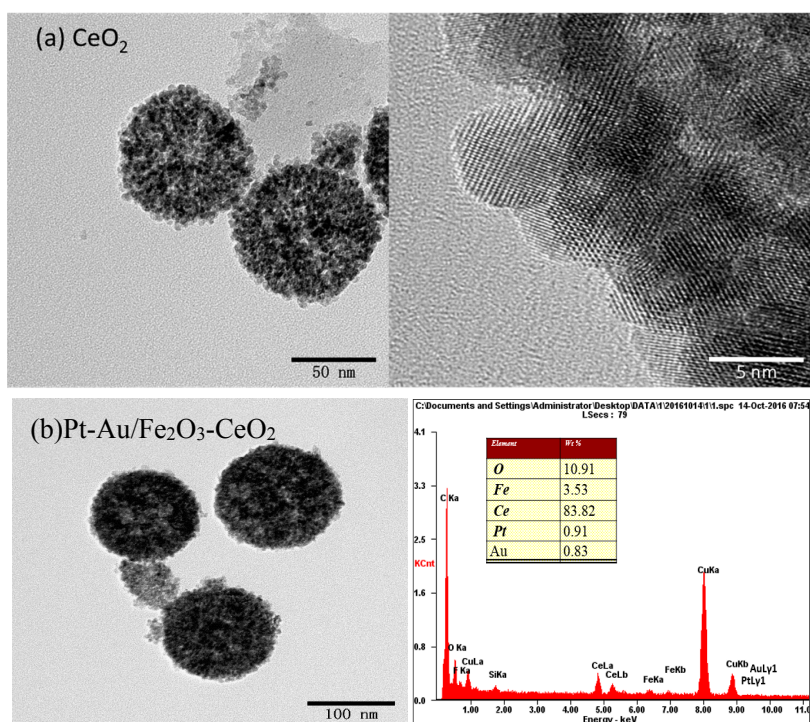
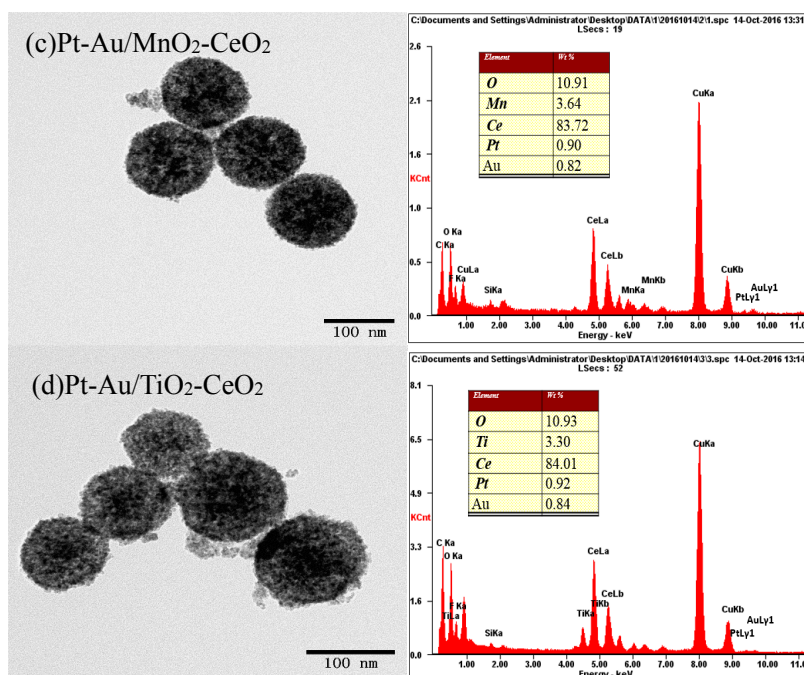


Figure 3. Cont.

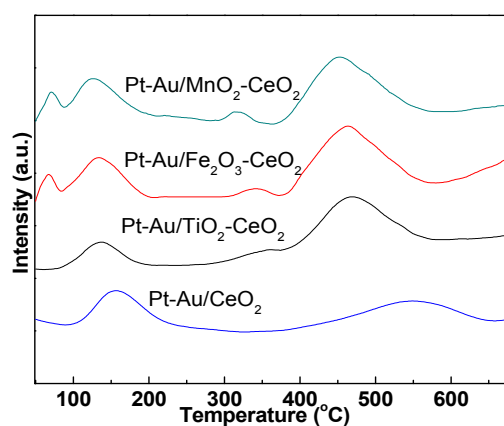


**Figure 3.** TEM image of the CeO<sub>2</sub> support and EDS results of Pt-Au/MO<sub>x</sub>-CeO<sub>2</sub> catalysts: (a) Pt-Au/CeO<sub>2</sub>; (b) Pt-Au/Fe<sub>2</sub>O<sub>3</sub>-CeO<sub>2</sub>; (c) Pt-Au/MnO<sub>2</sub>-CeO<sub>2</sub>; (d) Pt-Au/TiO<sub>2</sub>-CeO<sub>2</sub>.

Figure 4 shows the H<sub>2</sub>-TPR profiles of Pt-Au/MO<sub>x</sub>-CeO<sub>2</sub> catalysts. The reduction temperatures of Pt species are 70–100 °C [42]; Au species reduction temperatures are usually 100–200 °C [43]; and pure CeO<sub>2</sub> reduction temperature is around 553 °C [44]. The peak at 350 °C is attributed to the reduction of CeO<sub>2</sub> surface oxygen [45]. Evidently, no reduction peaks ascribed to Pt species are observed for Pt-Au/CeO<sub>2</sub> and Pt-Au/TiO<sub>2</sub>-CeO<sub>2</sub> catalysts, suggesting that all the Pt species are metallic Pt species. For Pt-Au/MnO<sub>2</sub>-CeO<sub>2</sub> and Pt-Au/Fe<sub>2</sub>O<sub>3</sub>-CeO<sub>2</sub> catalysts, the reduction peak at 75 °C is attributed to Pt<sup>2+</sup> species. For Pt-Au/CeO<sub>2</sub> catalyst, there are two reduction peaks at 160 and 553 °C, which are ascribed to the reduction peaks of Au species and CeO<sub>2</sub>, respectively [46]. Three reduction peaks at 146, 350 and 465 °C are observed for Pt-Au/TiO<sub>2</sub>-CeO<sub>2</sub> catalyst. It can be observed that three reduction peaks are at 144, 341 and 450 °C for Pt-Au/MnO<sub>2</sub>-CeO<sub>2</sub> catalyst. The reduction peaks are centered at 145, 350 and 464 °C for Pt-Au/Fe<sub>2</sub>O<sub>3</sub>-CeO<sub>2</sub> catalyst. It is worth noting that the reduction temperature of CeO<sub>2</sub> in Pt-Au/MO<sub>x</sub>-CeO<sub>2</sub> is lower than that of Pt-Au/CeO<sub>2</sub> nearly by 100 °C, which means that the oxidative performance of CeO<sub>2</sub> in Pt-Au/MO<sub>x</sub>-CeO<sub>2</sub> is higher than that of Pt-Au/CeO<sub>2</sub>. On the other hand, the introduction of MO<sub>x</sub> influences the reduction temperature of Au species. Lower reduction temperature of Au species indicates the active oxygen species formed on the Pt-Au/MO<sub>x</sub>-CeO<sub>2</sub> catalysts are more active [43]. It is very interesting that, even though the Pt species should be metallic Pt due to the reduction of NaBH<sub>4</sub> over the Pt-Au/MnO<sub>2</sub>-CeO<sub>2</sub> and Pt-Au/Fe<sub>2</sub>O<sub>3</sub>-CeO<sub>2</sub> catalysts, Pt<sup>2+</sup> species is observed. The presence of Pt<sup>2+</sup> species can be caused by the addition of MnO<sub>2</sub> and Fe<sub>2</sub>O<sub>3</sub>, both of which improve the electron transfer from Pt sites to CeO<sub>2</sub>, thus leading to the oxidation of metallic Pt species to Pt<sup>2+</sup> species. Metallic Pt species are more active than Pt<sup>2+</sup> species for the oxidation reaction, which may clarify the poor activities of Pt-Au/MnO<sub>2</sub>-CeO<sub>2</sub> catalyst and Pt-Au/Fe<sub>2</sub>O<sub>3</sub>-CeO<sub>2</sub> catalyst for the H<sub>2</sub> oxidation. H<sub>2</sub> consumed amounts are 0.21, 0.31, 0.38 and 0.39 mmol<sup>-1</sup> for the Pt-Au/CeO<sub>2</sub>, Pt-Au/TiO<sub>2</sub>-CeO<sub>2</sub>, Pt-Au/Fe<sub>2</sub>O<sub>3</sub>-CeO<sub>2</sub>, and Pt-Au/MnO<sub>2</sub>-CeO<sub>2</sub> catalysts, respectively. It indicates that the addition of MO<sub>x</sub> can promote the redox property of Pt-Au/CeO<sub>2</sub> catalyst.

**Table 1.** Chemical composition and textural properties of Pt-Au/MO<sub>x</sub>-CeO<sub>2</sub> catalysts.

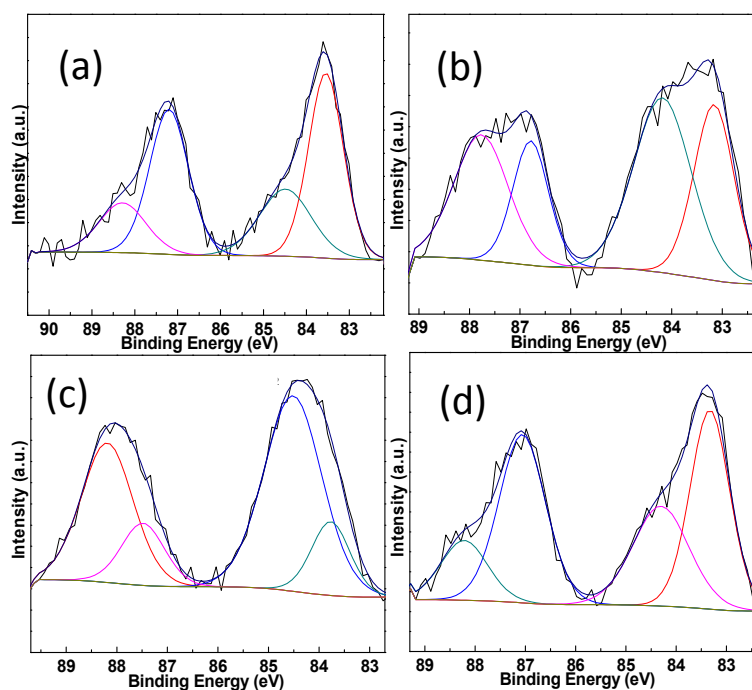
Catalyst	BET Surface Area (m <sup>2</sup> /g)	Dispersion of Noble Metal	Surface Composition (wt %)	
			Pt	Au
Pt-Au/CeO <sub>2</sub>	156.4	56.3%	0.46	0.51
Pt-Au/Fe <sub>2</sub> O <sub>3</sub> -CeO <sub>2</sub>	125.8	55.7%	0.44	0.48
Pt-Au/MnO <sub>2</sub> -CeO <sub>2</sub>	119.7	55.1%	0.47	0.47
Pt-Au/TiO <sub>2</sub> -CeO <sub>2</sub>	131.3	55.7%	0.46	0.52

**Figure 4.** H<sub>2</sub>-TPR profiles of Pt-Au/MO<sub>x</sub>-CeO<sub>2</sub> catalysts.

XPS measurements are conducted on the Pt-Au/MO<sub>x</sub>-CeO<sub>2</sub> samples and the results are listed in Table 2. The peaks at 83.3–83.6 eV and 84.2–84.5 eV can be assigned to Au<sup>0</sup> species and Au<sup>+</sup> species, respectively [46,47]. The peaks at 70.2–70.8 eV and 72.4–72.6 eV are attributed to Pt<sup>0</sup> species and Pt<sup>2+</sup> species [48]. Figures 5 and 6 show that the addition of MO<sub>x</sub> influences the chemical states of Pt species and Au species due to the electron transfer from Au species and Pt species to CeO<sub>2</sub> [49–52]. Cationic Au species possess higher activity than metallic Au species on the CO oxidation [42]. Compared with Pt-Au/CeO<sub>2</sub> catalyst, the addition of MO<sub>x</sub> results in the presence of more cationic Au species over Pt-Au/MO<sub>x</sub>-CeO<sub>2</sub> catalysts. The Ce 3d XPS peaks were fitted by searching for the optimum combination of Gaussian bands with the correlation coefficients (*r*<sup>2</sup>) above 0.99. In Figure 7, the Ce 3d core level spectra of the catalyst can be divided into eight components and the content of Ce<sup>3+</sup> are listed in Table 2. The bands labeled *u'* and *v'* represent the 3d<sup>10</sup>4f<sup>1</sup> corresponding to Ce<sup>3+</sup>, and the bands labeled *u*, *u''*, *u'''*, *v*, *v''*, and *v'''* represent the 3d<sup>10</sup>4f<sup>0</sup> corresponding to Ce<sup>4+</sup> [53]. Among Pt-Au/MO<sub>x</sub>-CeO<sub>2</sub> catalysts, the content of Ce<sup>3+</sup> over Pt-Au/MnO<sub>2</sub>-CeO<sub>2</sub> catalyst is the highest, indicating that more surface oxygen vacancies exist on Pt-Au/MnO<sub>2</sub>-CeO<sub>2</sub> catalyst. Previous researches showed that the formation of Ce<sup>3+</sup> over Au/CeO<sub>2</sub> catalysts was due to the charge transfer between Au sites and CeO<sub>2</sub> [49–51]. Therefore, the introduction of MO<sub>x</sub> enhances the charge transfer from Au species and Pt species to CeO<sub>2</sub> and leads to high content of cationic Au species. O1s XPS spectra of Pt-Au/MO<sub>x</sub>-CeO<sub>2</sub> catalysts are shown in Figure 8 and two peaks at 529.1–529.4 and 531.1–531.4 eV, respectively, appear. The former is ascribed to lattice oxygen (O<sub>I</sub>) and the latter is attributed to chemisorbed oxygen (O<sub>II</sub>) [47]. O<sub>II</sub> ratios [O<sub>II</sub>/(O<sub>II</sub> + O<sub>I</sub>)] over Pt-Au/MO<sub>x</sub>-CeO<sub>2</sub> catalysts are higher than that over Pt-Au/CeO<sub>2</sub> catalysts due to the presence of higher Ce<sup>3+</sup> content.

**Table 2.** XPS data analysis of Pt-Au/MO<sub>x</sub>-CeO<sub>2</sub> catalysts.

Catalyst	Pt Species	Content (at. %)	Au Species	Content (at. %)	Ce <sup>3+</sup> Species Content (at. %)
Pt-Au/CeO <sub>2</sub>	Pt <sup>2+</sup> (72.5 eV)	0	Au <sup>0</sup> (83.7 eV)	66.6	34.7
	Pt <sup>0</sup> (70.7 eV)	100	Au <sup>+</sup> (84.5 eV)	33.4	
Pt-Au/Fe <sub>2</sub> O <sub>3</sub> -CeO <sub>2</sub>	Pt <sup>0</sup> (70.7 eV)	77.7	Au <sup>0</sup> (83.6 eV)	44.4	40.9
	Pt <sup>2+</sup> (72.5 eV)	23.3	Au <sup>+</sup> (84.5 eV)	55.6	
Pt-Au/MnO <sub>2</sub> -CeO <sub>2</sub>	Pt <sup>0</sup> (70.7 eV)	67.5	Au <sup>0</sup> (83.6 eV)	18.4	41.1
	Pt <sup>2+</sup> (72.5 eV)	32.5	Au <sup>+</sup> (84.5 eV)	81.6	
Pt-Au/TiO <sub>2</sub> -CeO <sub>2</sub>	Pt <sup>2+</sup> (72.5 eV)	0	Au <sup>0</sup> (83.4 eV)	59.2	36.7
	Pt <sup>0</sup> (70.7 eV)	100	Au <sup>+</sup> (84.5 eV)	40.8	

**Figure 5.** Au 4f XPS spectra of Pt-Au/MO<sub>x</sub>-CeO<sub>2</sub> catalysts: (a) Pt-Au/CeO<sub>2</sub>; (b) Pt-Au/Fe<sub>2</sub>O<sub>3</sub>-CeO<sub>2</sub>; (c) Pt-Au/MnO<sub>2</sub>-CeO<sub>2</sub>; (d) Pt-Au/TiO<sub>2</sub>-CeO<sub>2</sub>.

To further understand the relationship between catalyst activity and catalyst physicochemical property, In-situ diffuse reflectance infrared Fourier transform spectroscopy (In-situ DRIFT) spectra of the Pt-Au/MO<sub>x</sub>-CeO<sub>2</sub> catalysts obtained upon exposure to CO, H<sub>2</sub> and synthetic air at 25 °C are shown in Figure 9. Seven distinct bands are observed in the in-situ DRIFT spectra. The bands at 3324–3395, 1640, 3691–3701, 2169, 2083–2084, 1568–1575, and 1282–1298 cm<sup>-1</sup> are ascribed to isolated hydroxyl groups  $\nu(\text{OH})$  [29], adsorbed water  $\delta(\text{H-O-H})$  [43], another hydroxyl groups  $\nu(\text{OH})$  [54–58], the adsorption of CO on Au sites [59–61], the adsorption of CO on Pt sites [42,62,63], the carbonate species [29], and carbonate species [29], respectively. It has been proposed that isolated hydroxyl groups originated from the decomposition of the OOH species, which were generated from the reaction between the associatively adsorbed oxygen and dissociative adsorbed hydrogen, and the isolated hydroxyl groups further react with dissociative adsorbed hydrogen to generate H<sub>2</sub>O [7,29].

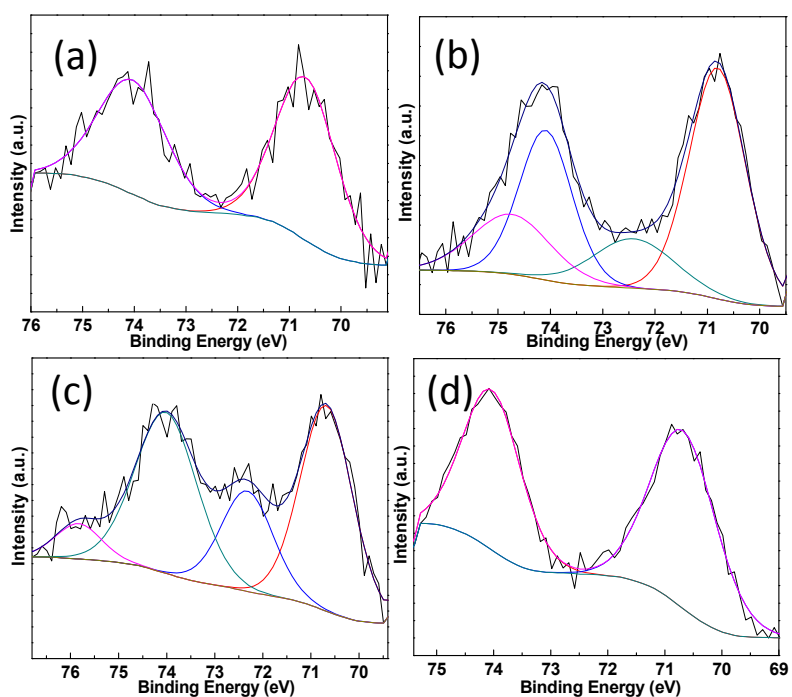


**Figure 6.** Pt 4f XPS spectra of Pt-Au/ $\text{MO}_x$ - $\text{CeO}_2$  catalysts: (a) Pt-Au/ $\text{CeO}_2$ ; (b) Pt-Au/ $\text{Fe}_2\text{O}_3$ - $\text{CeO}_2$ ; (c) Pt-Au/ $\text{MnO}_2$ - $\text{CeO}_2$ ; (d) Pt-Au/ $\text{TiO}_2$ - $\text{CeO}_2$ .

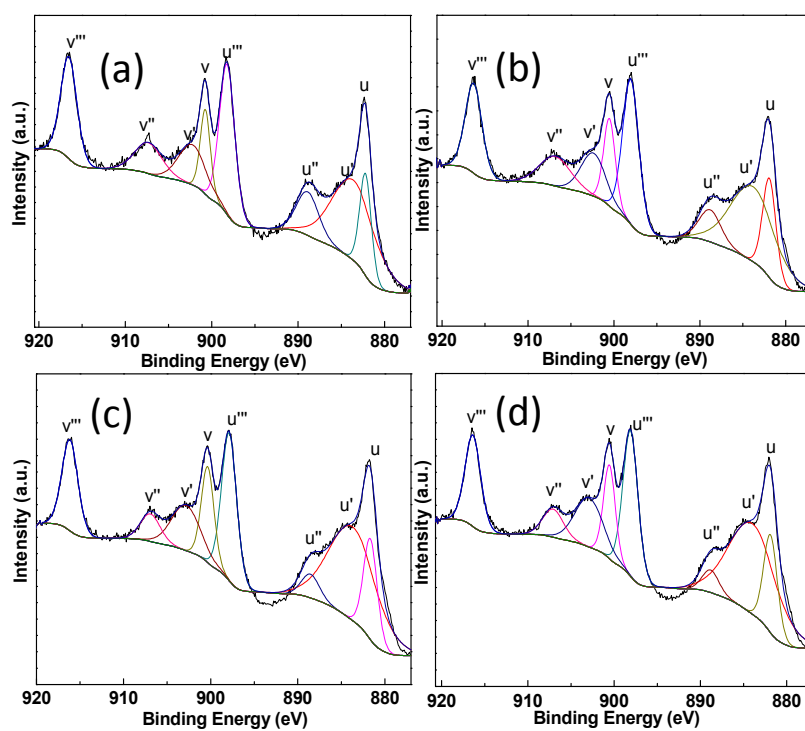


**Figure 7.** Ce 3d XPS spectra of Pt-Au/ $\text{MO}_x$ - $\text{CeO}_2$  catalysts: (a) Pt-Au/ $\text{CeO}_2$ ; (b) Pt-Au/ $\text{TiO}_2$ - $\text{CeO}_2$ ; (c) Pt-Au/ $\text{Fe}_2\text{O}_3$ - $\text{CeO}_2$ ; (d) Pt-Au/ $\text{MnO}_2$ - $\text{CeO}_2$ .

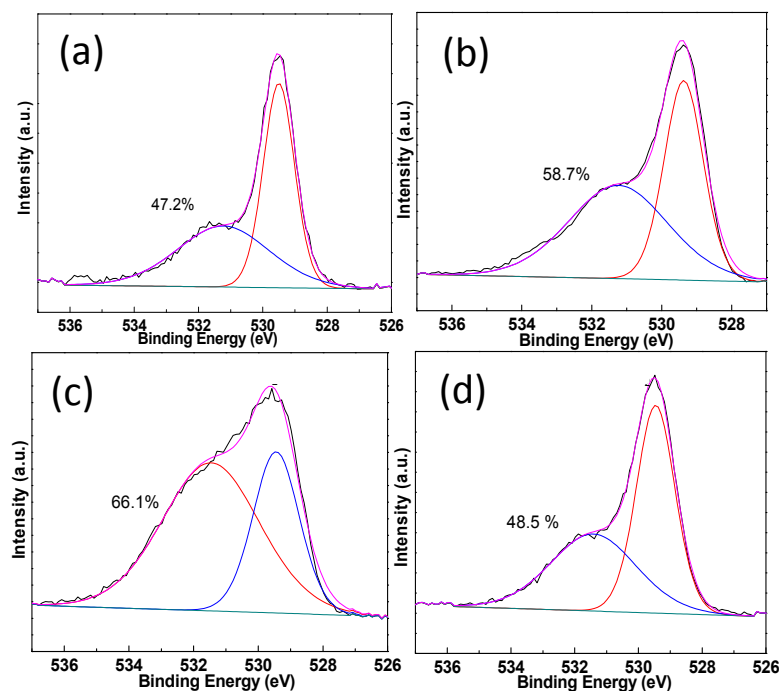


**Figure 8.** O1s XPS spectra and O<sub>II</sub> ratios of Pt-Au/MO<sub>x</sub>-CeO<sub>2</sub> catalysts: (a) Pt-Au/CeO<sub>2</sub>; (b) Pt-Au/Fe<sub>2</sub>O<sub>3</sub>-CeO<sub>2</sub>; (c) Pt-Au/MnO<sub>2</sub>-CeO<sub>2</sub>; (d) Pt-Au/TiO<sub>2</sub>-CeO<sub>2</sub>.

Intensity of reactant-related is due to reactant oxidation and reactant adsorption capability. To solve this problem, In-situ DRIFTS test results of Pt-Au/CeO<sub>2</sub> catalyst upon 3000 ppm CO + N<sub>2</sub> and 3000 ppm CO + 3000 pm H<sub>2</sub> + synthetic air can be observed in the Figure 10. The results indicate that the CO accumulation amount does not reach the CO saturated adsorption capability over Pt-Au/CeO<sub>2</sub> catalyst upon 3000 ppm CO + 3000 pm H<sub>2</sub> + synthetic air. CO saturated adsorption capability of Pt-Au/MO<sub>x</sub>-CeO<sub>2</sub> catalysts may be close to that of Pt-Au/CeO<sub>2</sub> catalyst due to the close amount of Pt and Au species over Pt-Au/CeO<sub>2</sub> catalyst and Pt-Au/MO<sub>x</sub>-CeO<sub>2</sub> catalysts. Little CO accumulation on Pt-Au/MO<sub>x</sub>-CeO<sub>2</sub> catalysts in Figure 9 is because of the enhanced CO oxidation instead of adsorption capability. For Pt-Au/CeO<sub>2</sub> catalyst, the intensity of bands at 2169 and 2084 cm<sup>-1</sup> increases, which means that much CO accumulates on the Au and Pt active sites. The intensity of other bands are almost unchanged, which suggests little H<sub>2</sub> is oxidized because Pt active sites are occupied and poisoned by CO. Therefore, CO and H<sub>2</sub> cannot be simultaneously removed over Pt-Au/CeO<sub>2</sub> catalyst. For Pt-Au/MnO<sub>2</sub>-CeO<sub>2</sub> catalyst, no peaks can be observed at 2169 and 2084 cm<sup>-1</sup> with the reaction proceeding, which suggests that the introduction of MnO<sub>2</sub> enhances the oxidation of CO. However, the intensity of bands at 3389 and 1640 cm<sup>-1</sup> are seldom unchanged, which indicates that little H<sub>2</sub> is oxidized. Therefore, the introduction of MnO<sub>2</sub> improves the oxidation of CO but not the oxidation of H<sub>2</sub>. Over Pt-Au/Fe<sub>2</sub>O<sub>3</sub>-CeO<sub>2</sub> catalyst, the intensity of the peak at 2084 cm<sup>-1</sup> suggests that little CO accumulates and the Fe<sub>2</sub>O<sub>3</sub> improves the activity of Pt-Au/CeO<sub>2</sub> catalyst for CO oxidation. The intensity of bands at 3386 and 1640 cm<sup>-1</sup> suggest that little H<sub>2</sub> is oxidized to H<sub>2</sub>O. Consequently, Fe<sub>2</sub>O<sub>3</sub> improves the activity of Pt-Au/CeO<sub>2</sub> catalyst for the CO oxidation not for H<sub>2</sub> oxidation. Some CO accumulates on the Pt-Au/TiO<sub>2</sub>-CeO<sub>2</sub> catalyst, as confirmed by the presence of the band at 2084 cm<sup>-1</sup>. The intensity change of peaks at 3691, 3395 and 1640 cm<sup>-1</sup> suggests that many isolated -OH species and H<sub>2</sub>O are produced, indicating that much H<sub>2</sub> is oxidized into H<sub>2</sub>O. Based on the in-situ DRIFTS results of the Pt-Au/MO<sub>x</sub>-CeO<sub>2</sub> catalysts, Pt-Au/TiO<sub>2</sub>-CeO<sub>2</sub> catalyst presents the best catalytic activity for the co-oxidation of CO and H<sub>2</sub>.

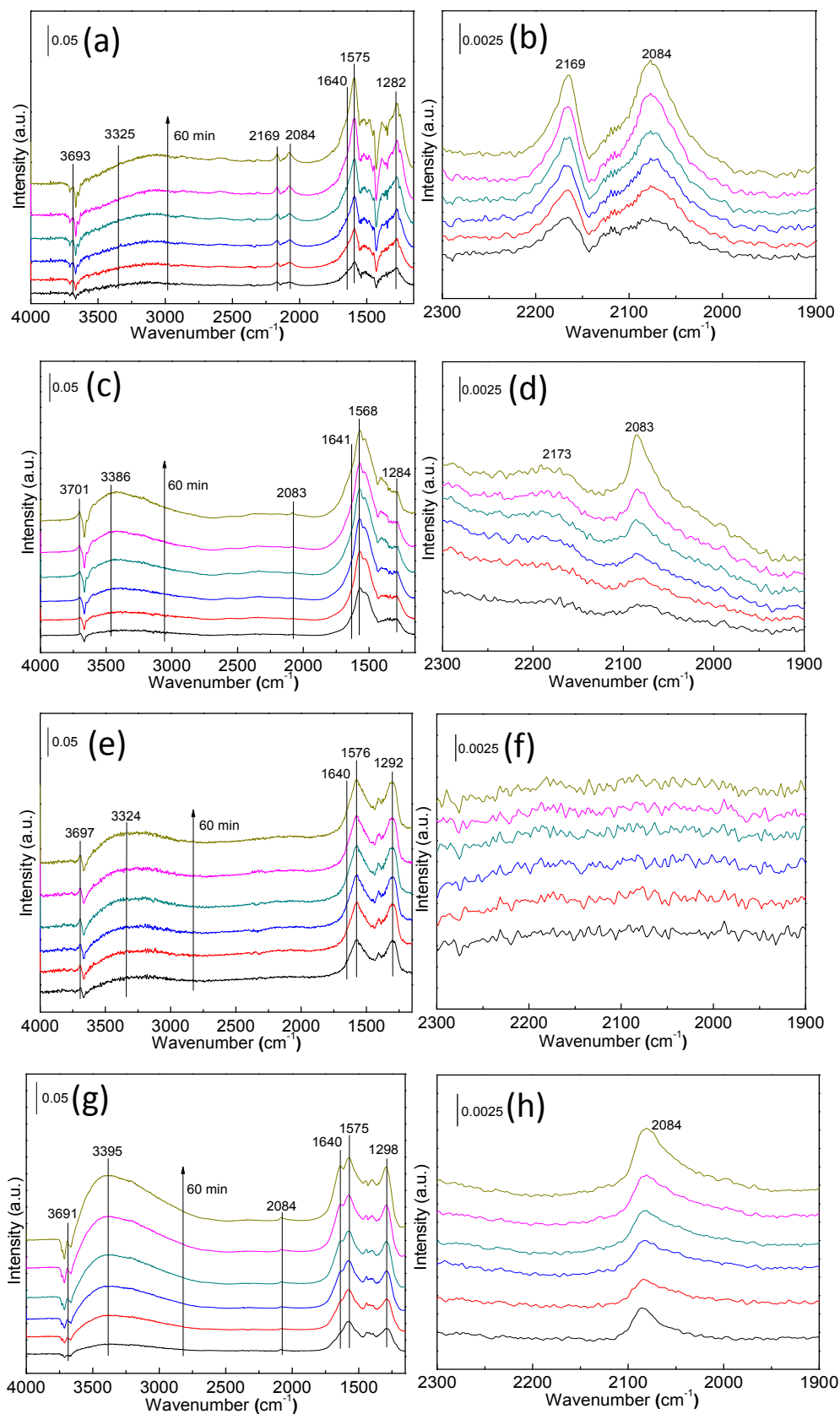


**Figure 9.** In-situ DRIFT spectra of the Pt-Au/MO<sub>x</sub>-CeO<sub>2</sub> catalysts after exposed upon 3000 ppm CO + 3000 ppm H<sub>2</sub> + synthetic air for 60 min at 25 °C: (a,b) Pt-Au/CeO<sub>2</sub>; (c,d) Pt-Au/Fe<sub>2</sub>O<sub>3</sub>-CeO<sub>2</sub>; (e,f) Pt-Au/MnO<sub>2</sub>-CeO<sub>2</sub>; (g,h) Pt-Au/TiO<sub>2</sub>-CeO<sub>2</sub>.

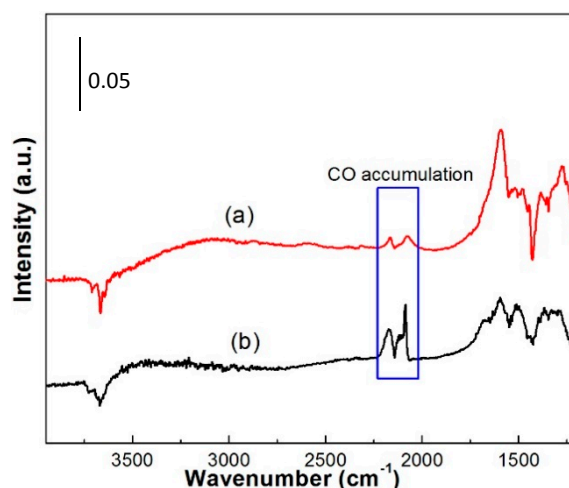


**Figure 10.** In-situ DRIFTS spectra of the Pt-Au/CeO<sub>2</sub> catalysts after exposed upon: (a) 3000 ppm CO + 3000 ppm H<sub>2</sub> + synthetic air; and (b) 3000 ppm CO + N<sub>2</sub> for 60 min at 25 °C.

Figure 11 shows the effect of CO concentration on the co-oxidation of CO and H<sub>2</sub> through in-situ DRIFTS. The intensity of the bands at 3395 and 1640 cm<sup>-1</sup> in Figure 11b are stronger than that shown in Figure 11a, indicating that more H<sub>2</sub>O are produced. Therefore, CO obviously hinders the oxidation of H<sub>2</sub> in the co-oxidation of CO and H<sub>2</sub>, which is in accordance with previous reports [22].

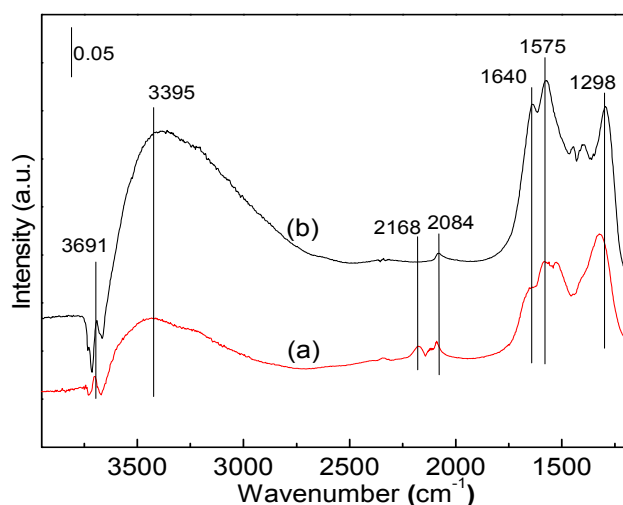


**Figure 11.** In-situ DRIFTS spectra over Pt-Au/TiO<sub>2</sub>-CeO<sub>2</sub> catalysts after exposed upon: (a) 5000 ppm CO + 3000 ppm H<sub>2</sub> + synthetic air; and (b) 3000 ppm CO + 3000 ppm H<sub>2</sub> + synthetic air for 60 min at 25 °C.

### 3. Materials and Methods

#### 3.1. Catalyst Preparation

The CeO<sub>2</sub> nanospheres were prepared by hydrothermal method. Thirteen grams Ce(NO<sub>3</sub>)<sub>3</sub>·6H<sub>2</sub>O was dissolved in 13 mL ultra-pure water at room temperature. Then, 13 mL propionic acid and 390 mL ethylene glycol were added under stirring to form a uniform solution at room temperature. The uniform solution was transferred to a Teflon-sealed autoclave and heated at 180 °C for 7.5 h. After the hydrothermal treatment, the mixture was centrifuged and washed with ethanol for several times. The obtained solid was dried at 100 °C overnight, subsequently it was calcined in air at 400 °C for 4 h. Then CeO<sub>2</sub> nanospheres were obtained.

$\text{MO}_x\text{-CeO}_2$  ( $M = \text{Mn, Fe, Ti}$ ) supports, with a  $\text{Ce}/M$  molar ratio of 9, were obtained by precipitation method.  $\text{CeO}_2$  nanospheres were homogeneously dispersed in  $\text{Mn}(\text{NO}_3)_2$  or  $\text{Fe}(\text{NO}_3)_3$  aqueous solution, or *tetra-n*-butyl titanate ethanol solution, and the suspension was stirred for 2 h at room temperature. Then ammonia solution was added to the above solution under stirring until pH was 10 at room temperature. The suspension was filtered and washed with ultra-pure water. The obtained solid samples were first dried at 105 °C for 12 h and subsequently calcined in air at 400 °C for 4 h to obtain  $\text{MO}_x\text{-CeO}_2$  ( $M = \text{Mn, Fe, Ti}$ ) supports.

$\text{Pt-Au}/\text{MO}_x\text{-CeO}_2$  ( $M = \text{Mn, Fe, Ti}$ ) catalysts were prepared by reduction-deposition precipitation method [49]. Four grams  $\text{MO}_x\text{-CeO}_2$  was uniformly dispersed into the  $\text{H}_2\text{PtCl}_6$  solution containing 0.04 g Pt at room temperature. After impregnation for 2 h, the pH value of suspension was adjusted to 10.  $\text{NaBH}_4$  solution was quickly added into the suspension ( $\text{NaBH}_4/\text{Pt} = 10$ , molar ratio) while being stirred for 2 h at room temperature. The suspension was filtered and washed with ultra-pure water, then dried under vacuum at 120 °C for 12 h to obtain  $\text{Pt}/\text{MO}_x\text{-CeO}_2$ . Then 2 g  $\text{Pt}/\text{MO}_x\text{-CeO}_2$  was uniformly dispersed into the  $\text{HAuCl}_4$  solution containing 0.02 g Au at room temperature. Subsequently, urea was added as the precipitant. The mixture was stirred at 80 °C for 8 h and then aged for 12 h at room temperature. Then, the mixture was filtered and washed with ultra-pure water. The resulting powder was dried under vacuum at room temperature for 12 h to yield  $\text{Pt-Au}/\text{MO}_x\text{-CeO}_2$  catalysts.

### 3.2. Catalyst Characterization

XRD patterns were recorded with a Shimadzu (Tokyo, Japan) XRD-6000 diffractometer operated at 40 kV and 40 mA, using nickel-filtered  $\text{Cu K}\alpha$  ( $\lambda = 0.1542$  nm) radiation. Surface areas of the catalysts were determined by the BET method by a Micromeritics ASAP 2000 instrument (Quantachrome, Boynton Beach, FL, USA). CO chemisorption measurements were measured an Autochem II 2920 (Micromeritics Instrument Corp, Atlanta, GA, USA) automated chemisorption analyzer. The surface chemical states of  $\text{Pt-Au}/\text{MO}_x\text{-CeO}_2$  catalysts were tested by XPS (PHI Quantro SXM ULVAC-PHI, Tokyo, Japan) using an  $\text{Al K}\alpha$  X-ray source (1486.7 eV) at 15 kV and 25 W with the binding energy calibrated by C 1s at 284.8 eV. HRTEM micrographs were obtained with a JEM-2100F (Jeol, Tokyo, Japan) microscope at 200 kV.

$\text{H}_2$ -TPR measurements equipped with a quadrupole mass spectrometer (Omnistar, Atlanta, GA, USA, GSD-301-O2) were carried out in a fixed bed microreactor. The 0.2-g sample was pretreated under Ar at 120 °C for 1 h. After cooled to 25 °C, the catalyst was reduced under 5%  $\text{H}_2/\text{N}_2$  gas flow ( $50 \text{ mL min}^{-1}$ ) within the temperature of 30 to 700 °C at  $10 \text{ }^\circ\text{C min}^{-1}$ . In-situ DRIFTS were recorded in a Nicolet 6700 FTIR spectrometer (Nicolet, Atlanta, GA, USA). Before characterization, all the catalysts were pretreated under Ar at a flow rate of  $100 \text{ mL min}^{-1}$  at 120 °C for 0.5 h. After cooled to 25 °C, the reactant gas mixture, comprised of 1000 ppm  $\text{H}_2$ , 1000 ppm CO and synthetic air (50% relative humidity), was introduced into the DRIFT cell at a flow rate of  $100 \text{ mL min}^{-1}$ . All spectra were recorded by accumulating 32 scans with a resolution of  $4 \text{ cm}^{-1}$ .

### 3.3. Catalytic Activity Measurement

The activity evaluation for the co-oxidation of CO and  $\text{H}_2$  was performed in a continuous flow fixed-bed quartz reactor (i.d. = 10 mm) by using 0.36 g catalyst at 25 °C. Before activity evaluation, the  $\text{Pt-Au}/\text{MO}_x\text{-CeO}_2$  catalysts were pretreated under Ar at 120 °C for 0.5 h at a flow rate of  $100 \text{ mL}\cdot\text{min}^{-1}$ . The simultaneous reaction gas consisted of 100 ppm CO and 480 ppm  $\text{H}_2$ , and air (50% relative humidity) as the balance gas, and the total flow rate was fixed at  $3.6 \text{ L}\cdot\text{min}^{-1}$ , corresponding to a GHSV of  $500,000 \text{ h}^{-1}$ .  $\text{H}_2$ , CO and  $\text{CO}_2$  were measured by gas chromatograph (GC) equipped with TCD and FID detectors. CO and  $\text{CO}_2$  were converted to  $\text{CH}_4$  by Ni catalytic converter before the measurement.

## 4. Conclusions

A series of nanostructured  $\text{Pt-Au}/\text{MO}_x\text{-CeO}_2$  ( $M = \text{Mn, Fe, Ti}$ ) catalysts were prepared and  $\text{Pt-Au}/\text{TiO}_2\text{-CeO}_2$  catalyst presented the best catalytic performance for the total co-oxidation of CO

and H<sub>2</sub> at room temperature. The introduction of MO<sub>x</sub> into CeO<sub>2</sub> can enhance the charge transfer from Pt and Au sites to CeO<sub>2</sub>, which improves CO oxidation. The introduction of TiO<sub>2</sub> enhances the decomposition of OOH species into O species and OH species, while the introduction of MnO<sub>2</sub> and Fe<sub>2</sub>O<sub>3</sub> cannot. The addition of TiO<sub>2</sub> mainly accounts for the high activity for the co-oxidation of CO and H<sub>2</sub> over the Pt-Au/TiO<sub>2</sub>-CeO<sub>2</sub> catalyst.

**Acknowledgments:** This work has been financially supported by the National Natural Science Foundation of China (21177006) and Special Foundation for Environmental Public Sector Research of Ministry of Environmental Protection of People's Republic of China (No. 201409080).

**Author Contributions:** Tianle Zhu and Zhiming Liu conceived and designed the experiments; Xiaowei Hong and Ye Sun performed the experiments, analyzed the data and wrote the paper.

**Conflicts of Interest:** The authors declare no conflict of interest.

## References

1. Seo, P.W.; Choi, H.J.; Hong, S.I.; Hong, S.C. A study on the characteristics of CO oxidation at room temperature by metallic Pt. *J. Hazard. Mater.* **2010**, *178*, 917–925. [[CrossRef](#)] [[PubMed](#)]
2. Tang, X.F.; Chen, J.L.; Huang, X.M.; Xu, Y.; Shen, W.J. Pt/MnO<sub>x</sub>-CeO<sub>2</sub> catalysts for the complete oxidation of formaldehyde at ambient temperature. *Appl. Catal. B* **2008**, *81*, 115–121. [[CrossRef](#)]
3. Noei, H.; Qiu, H.; Wang, Y.; Muhler, M.; Wöll, C. Hydrogen loading of oxide powder particles: A transmission IR study for the case of zinc oxide. *ChemPhysChem* **2010**, *11*, 3604–3607. [[CrossRef](#)] [[PubMed](#)]
4. Reina, T.R.; Moreno, A.A.; Ivanova, S.; Odriozola, J.A.; Centeno, M.A. Influence of Vanadium or Cobalt Oxides on the CO Oxidation Behavior of Au/MO<sub>x</sub>/CeO<sub>2</sub>-Al<sub>2</sub>O<sub>3</sub> Systems. *ChemCatChem* **2012**, *4*, 512–520. [[CrossRef](#)]
5. Qiao, B.; Wang, A.Q.; Takahashi, M.; Zhang, Y.J.; Wang, J.H.; Deng, Y.Q.; Zhang, T. A novel Au & Pd/Fe(OH)<sub>(x)</sub> catalyst for CO + H<sub>2</sub> co-oxidations at low temperatures. *J. Catal.* **2011**, *279*, 361–365.
6. Liu, P.; Logadottir, A.; Nørskov, J.K. Modeling the electro-oxidation of CO and H<sub>2</sub>/CO on Pt, Ru, PtRu and Pt<sub>3</sub>Sn. *Electrochim. Acta* **2003**, *48*, 3731–3742.
7. Green, I.X.; Tang, W.; Neurock, M.; Yates, J.T. Low-Temperature Catalytic H<sub>2</sub> oxidation over Au Nanoparticle/TiO<sub>2</sub> Dual Perimeter Sites. *Angew. Chem. Int. Ed.* **2011**, *50*, 10186–10189. [[CrossRef](#)] [[PubMed](#)]
8. Javier, G.; Silvio, C.; Fierro-Gonzalez, J.C.; Hao, Y.; Gates, B.C.; Avelino, C. CO oxidation catalyzed by supported gold: cooperation between gold and nanocrystalline rare-earth supports forms reactive surface superoxide and peroxide species. *Angew. Chem. Int. Ed.* **2005**, *117*, 4778–4781.
9. Ramirez-Alvarez, E.; Rico-Martinez, R.; Krischer, K. Self-organized reactivity patterns during the oxidation of H<sub>2</sub>-CO mixtures on a rotating Pt ring-electrode. *Electrochim. Acta* **2013**, *112*, 894–898. [[CrossRef](#)]
10. Giorgi, L.; Pozio, A.; Bracchini, C.; Giorgi, R.; Turtù, S. H<sub>2</sub> and H<sub>2</sub>/CO oxidation mechanism on Pt/C, Ru/C and Pt-Ru/C electrocatalysts. *J. Appl. Electrochem.* **2001**, *31*, 325–334. [[CrossRef](#)]
11. Arenz, M.; Stamenkovic, V.; Blizanac, B.B.; Mayrhofer, K.J.J.; Markovic, N.M.; Ross, P.N. Carbon-supported Pt-Sn electrocatalysts for the anodic oxidation of H<sub>2</sub>, CO, and H<sub>2</sub>/CO mixtures. Part II: The structure-activity relationship. *J. Catal.* **2005**, *232*, 402–410. [[CrossRef](#)]
12. Li, Z.H.; Yang, K.; Liu, G.; Deng, G.F.; Li, J.Q.; Li, G.; Yue, R.L.; Yang, J.; Chen, Y.F. Effect of Reduction Treatment on Structural Properties of TiO<sub>2</sub> Supported Pt Nanoparticles and Their Catalytic Activity for Benzene Oxidation. *Catal. Lett.* **2014**, *144*, 1080–1087. [[CrossRef](#)]
13. Huang, H.; Leung, D.Y.C.; Ye, D. Effect of reduction treatment on structural properties of TiO<sub>2</sub> supported Pt nanoparticles and their catalytic activity for formaldehyde oxidation. *J. Mater. Chem.* **2011**, *21*, 9647–9652. [[CrossRef](#)]
14. Hutchings, G.J. Catalysis by gold. *Catal. Today* **2005**, *100*, 55–61. [[CrossRef](#)]
15. Carrettin, S.; Concepcion, P.; Corma, A.; Lopez Nieto, J.M.; Puentes, V.F. Nanocrystalline CeO<sub>2</sub> increases the activity of Au for CO oxidation by two orders of magnitude. *Angew. Chem. Int. Ed.* **2004**, *43*, 2538–2540. [[CrossRef](#)] [[PubMed](#)]
16. Yu, J.; Wu, G.S.; Lu, G.Z.; Mao, D.S.; Guo, Y. Promoting effects of ceria on the catalytic performance of gold supported on TiO<sub>2</sub> for low-temperature CO oxidation. *RSC Adv.* **2014**, *4*, 16985–16991. [[CrossRef](#)]

17. Wang, L.C.; Huang, X.S.; Liu, Q.; Liu, Y.M.; Cao, Y.; He, H.Y.; Fan, K.N.; Zhuang, J.H. Gold nanoparticles deposited on manganese(III) oxide as novel efficient catalyst for low temperature CO oxidation. *J. Catal.* **2008**, *259*, 66–74. [[CrossRef](#)]
18. Qiao, B.; Zhang, J.; Liu, L.; Deng, Y. Low-temperature prepared highly effective ferric hydroxide supported gold catalysts for carbon monoxide selective oxidation in the presence of hydrogen. *Appl. Catal. A* **2008**, *340*, 220–228. [[CrossRef](#)]
19. Hutchings, G.; Hall, M.; Carley, A.; Landon, P.; Solsona, B.; Kiely, C.; Herzing, A.; Makkee, M.; Moulijn, J.; Overweg, A. Role of gold cations in the oxidation of carbon monoxide catalyzed by iron oxide-supported gold. *J. Catal.* **2006**, *242*, 71–81. [[CrossRef](#)]
20. Avgouropoulos, G.; Ioannides, T. CO tolerance of Pt and Rh catalysts: effect of CO in the gas-phase oxidation of H<sub>2</sub> over Pt and Rh supported catalysts. *Appl. Catal. B* **2005**, *56*, 77–86. [[CrossRef](#)]
21. Liu, Y.; Liu, B.; Liu, Y.; Wang, Q.; Hu, W.; Jing, P.; Liu, L.; Yu, S.; Zhang, J. Improvement of catalytic performance of preferential oxidation of CO in H<sub>2</sub>-rich gases on three-dimensionally ordered macro- and meso-porous Pt–Au/CeO<sub>2</sub> catalysts. *Appl. Catal. B* **2013**, *142*, 615–625. [[CrossRef](#)]
22. Liu, L.Q.; Qiao, B.T.; He, Y.D.; Zhou, F.; Yang, B.Q.; Deng, Y.Q. Catalytic co-oxidation of CO and H<sub>2</sub> over FeO<sub>x</sub>-supported Pd catalyst at low temperatures. *J. Catal.* **2012**, *294*, 29–36. [[CrossRef](#)]
23. Alayoglu, S.; Nilekar, A.U.; Mavrikakis, M.; Eichhorn, B. Ru–Pt core–shell nanoparticles for preferential oxidation of carbon monoxide in hydrogen. *Nat. Mater.* **2008**, *7*, 333–338. [[CrossRef](#)] [[PubMed](#)]
24. Laguna, O.H.; Perez, A.; Centeno, M.A.; Odriozola, J.A. Synergy between gold and oxygen vacancies in gold supported on Zr-doped ceria catalysts for the CO oxidation. *Appl. Catal. B* **2015**, *176*, 385–395. [[CrossRef](#)]
25. Vayssilov, G.N.; Lykhach, Y.; Migani, A.; Staudt, T.; Petrova, G.P.; Tsud, N.; Skála, T.; Bruix, A.; Illas, F.; Prince, K.C. Support nanostructure boosts oxygen transfer to catalytically active platinum nanoparticles. *Nat. Mater.* **2011**, *10*, 310–315. [[CrossRef](#)] [[PubMed](#)]
26. Lykhach, Y.; Staudt, T.; Vorokhta, M.; Skála, T.; Johánek, V.; Prince, K.C.; Matolín, V.; Libuda, J. Hydrogen spillover monitored by resonant photoemission spectroscopy. *J. Catal.* **2012**, *285*, 6–9. [[CrossRef](#)]
27. Teschner, D.; Woosch, A.; Röder, T.; Matusek, K.; Paál, Z. Ceria as a new support of noble metal catalysts for hydrocarbon reactions: Chemisorption and catalytic studies. *Solid State Ionics* **2001**, *141*, 709–713. [[CrossRef](#)]
28. Khetan, A.; Pitsch, H.; Han, B. Structure and Reactivity of Sub-Monolayer Pt on CeO<sub>2</sub> Surface from First Principles Thermodynamics. *ESC Meet. Abstr.* **2014**, *122*, 153–164.
29. Piccolo, L.; Daly, H.; Valcarcel, A.; Meunier, F.C. Promotional effect of H<sub>2</sub> on CO oxidation over Au/TiO<sub>2</sub> studied by operando infrared spectroscopy. *Appl. Catal. B* **2009**, *86*, 190–195. [[CrossRef](#)]
30. Cao, J.L.; Wang, Y.; Yu, X.L.; Wang, S.R.; Wu, S.H.; Yuan, Z.Y. Mesoporous CuO–Fe<sub>2</sub>O<sub>3</sub> composite catalysts for low-temperature carbon monoxide oxidation. *Appl. Catal. B* **2008**, *79*, 26–34. [[CrossRef](#)]
31. Tabakova, T.; Avgouropoulos, G.; Papavasiliou, J.; Manzoli, M.; Boccuzzi, F.; Tenchev, K.; Vindigni, F.; Ioannides, T. CO-free hydrogen production over Au/CeO<sub>2</sub>–Fe<sub>2</sub>O<sub>3</sub> catalysts: Part 1. Impact of the support composition on the performance for the preferential CO oxidation reaction. *Appl. Catal. B* **2011**, *101*, 256–265. [[CrossRef](#)]
32. Zepeda, T.; Martínez-Hernández, A.; Guil-López, R.; Pawelec, B. Preferential CO oxidation in excess of hydrogen over Au/HMS catalysts modified by Ce, Fe and Ti oxides. *Appl. Catal. B* **2010**, *100*, 450–462. [[CrossRef](#)]
33. Peza-Ledesma, C.L.; Escamilla-Perea, L.; Nava, R.; Pawelec, B.; Fierro, J.L.G. Supported gold catalysts in SBA-15 modified with TiO<sub>2</sub> for oxidation of carbon monoxide. *Appl. Catal. A* **2010**, *375*, 37–48. [[CrossRef](#)]
34. Parreira, L.A.; Bogdanchikova, N.; Pestryakov, A.; Zepeda, T.A.; Tuzovskaya, I.; Fariás, M.H.; Gusevskaya, E.V. Nanocrystalline gold supported on Fe-, Ti- and Ce-modified hexagonal mesoporous silica as a catalyst for the aerobic oxidative esterification of benzyl alcohol. *Appl. Catal. A* **2011**, *397*, 145–152. [[CrossRef](#)]
35. Ayastuy, J.L.; González-Marcos, M.P.; González-Velasco, J.R.; Gutiérrez-Ortiz, M.A. MnO<sub>x</sub>/Pt/Al<sub>2</sub>O<sub>3</sub> catalysts for CO oxidation in H<sub>2</sub>-rich streams. *Appl. Catal. B* **2007**, *70*, 532–541. [[CrossRef](#)]
36. Zhao, Z.; Lin, X.; Jin, R.; Wang, G.; Muhammad, T. MO<sub>x</sub> (M = Mn, Fe, Ni or Cr) improved supported Co<sub>3</sub>O<sub>4</sub> catalysts on ceria–zirconia nanoparticulate for CO preferential oxidation in H<sub>2</sub>-rich gases. *Appl. Catal. B* **2012**, *115–116*, 53–62. [[CrossRef](#)]

37. Binas, V.D.; Sambani, K.; Maggos, T.; Katsanaki, A.; Kiriakidis, G. Synthesis and photocatalytic activity of Mn-doped TiO<sub>2</sub> nanostructured powders under UV and visible light. *Appl. Catal. B* **2012**, *113–114*, 79–86. [[CrossRef](#)]
38. Chang, S.M.; Liu, W.S. The roles of surface-doped metal ions (V, Mn, Fe, Cu, Ce, and W) in the interfacial behavior of TiO<sub>2</sub> photocatalysts. *Appl. Catal. B* **2014**, *156–157*, 466–475. [[CrossRef](#)]
39. Zanella, R.; Giorgio, S.; Henry, C.R.; Louis, C. Alternative methods for the preparation of gold nanoparticles supported on TiO<sub>2</sub>. *J. Phys. Chem. B* **2002**, *106*, 7634–7642. [[CrossRef](#)]
40. Daté, M.; Haruta, M. Moisture Effect on CO Oxidation over Au/TiO<sub>2</sub> Catalyst. *J. Catal.* **2001**, *201*, 221–224.
41. Xu, X.L.; Li, J.Q. DFT studies on H<sub>2</sub>O adsorption and its effect on CO oxidation over spinel Co<sub>3</sub>O<sub>4</sub> (110) surface. *Surf. Sci.* **2011**, *605*, 1962–1967. [[CrossRef](#)]
42. Na, H.; Zhu, T.; Liu, Z. Effect of preparation method on the performance of Pt–Au/TiO<sub>2</sub> catalysts for the catalytic co-oxidation of HCHO and CO. *Cata. Sci. Technol.* **2014**, *4*, 2051–2057.
43. Chen, B.B.; Shi, C.; Crocker, M.; Wang, Y.; Zhu, A.M. Catalytic removal of formaldehyde at room temperature over supported gold catalysts. *Appl. Catal. B* **2013**, *132–133*, 245–255. [[CrossRef](#)]
44. Wang, Y.; Zhu, A.; Zhang, Y.; Au, C.T.; Yang, X.; Shi, C. Catalytic reduction of NO by CO over NiO/CeO<sub>2</sub> catalyst in stoichiometric NO/CO and NO/CO/O<sub>2</sub> reaction. *Appl. Catal. B* **2008**, *81*, 141–149. [[CrossRef](#)]
45. Chen, Y.C.; Chen, K.B.; Lee, C.S.; Lin, M.C. Direct Synthesis of Zr-Doped Ceria Nanotubes. *J. Phys. Chem. C* **2009**, *113*, 5031–5034. [[CrossRef](#)]
46. Li, H.F.; Zhang, N.; Chen, P.; Luo, M.F.; Lu, J.Q. High surface area Au/CeO<sub>2</sub> catalysts for low temperature formaldehyde oxidation. *Appl. Catal. B* **2011**, *110*, 279–285. [[CrossRef](#)]
47. Hong, X.; Sun, Y.; Zhu, T.; Liu, Z. Pt-Au/CeO<sub>2</sub> catalysts for the simultaneous removal of carbon monoxide and formaldehyde. *Cata. Sci. Technol.* **2016**, *6*, 3606–3615. [[CrossRef](#)]
48. An, N.; Yu, Q.; Gang, L.; Li, S.; Jia, M.; Zhang, W. Complete oxidation of formaldehyde at ambient temperature over supported Pt/Fe<sub>2</sub>O<sub>3</sub> catalysts prepared by colloid-deposition method. *J. Hazard. Mater.* **2011**, *186*, 1392–1397. [[CrossRef](#)] [[PubMed](#)]
49. Lawrence, N.J.; Brewer, J.R.; Wang, L.; Wu, T.S.; Wells-Kingsbury, J.; Ihrig, M.M.; Wang, G.; Soo, Y.L.; Mei, W.N.; Cheung, C.L. Defect engineering in cubic cerium oxide nanostructures for catalytic oxidation. *Nano Lett.* **2011**, *11*, 2666–2671. [[CrossRef](#)] [[PubMed](#)]
50. Esch, F.; Fabris, S.; Zhou, L.; Montini, T.; Africh, C.; Fornasiero, P.; Comelli, G.; Rosei, R. Electron localization determines defect formation on ceria substrates. *Science* **2005**, *309*, 752–755. [[CrossRef](#)] [[PubMed](#)]
51. Kim, H.Y.; Lee, H.M.; Henkelman, G. CO oxidation mechanism on CeO<sub>2</sub>-supported Au nanoparticles. *J. Am. Chem. Soc.* **2012**, *134*, 1560–1570. [[CrossRef](#)] [[PubMed](#)]
52. Lykhach, Y.; Kozlov, S.M.; Skála, T.; Tovt, A.; Stetsovych, V.; Tsud, N.; Dvořák, F.; Johánek, V.; Neitzel, A.; Mysliveček, J. Counting electrons on supported nanoparticles. *Nat. Mater.* **2015**, *15*, 284–288. [[CrossRef](#)] [[PubMed](#)]
53. Shan, W.P.; Liu, F.D.; He, H.; Shi, X.Y.; Zhang, C.B. A superior Ce-W-Ti mixed oxide catalyst for the selective catalytic reduction of NO<sub>x</sub> with NH<sub>3</sub>. *Appl. Catal. B* **2012**, *115*, 100–106. [[CrossRef](#)]
54. Zhang, C.B.; Liu, F.D.; Zhai, Y.P.; Ariga, H.; Yi, N.; Liu, Y.C.; Asakura, K.; Flytzani-Stephanopoulos, M.; He, H. Alkali-Metal-Promoted Pt/TiO<sub>2</sub> Opens a More Efficient Pathway to Formaldehyde Oxidation at Ambient Temperatures. *Angew. Chem. Int. Ed.* **2012**, *51*, 9628–9632. [[CrossRef](#)] [[PubMed](#)]
55. Sun, S.; Ding, J.; Bao, J.; Gao, C.; Qi, Z.; Li, C. Photocatalytic oxidation of gaseous formaldehyde on TiO<sub>2</sub>: An in situ DRIFTS study. *Catal. Lett.* **2010**, *137*, 239–246. [[CrossRef](#)]
56. Enevoldsen, G.H.; Pinto, H.P.; Foster, A.S.; Jensen, M.C.; Hofer, W.A.; Hammer, B.; Lauritsen, J.V.; Besenbacher, F. Imaging of the hydrogen subsurface site in rutile TiO<sub>2</sub>. *Phys. Rev. Lett.* **2009**, *102*, 136103. [[CrossRef](#)] [[PubMed](#)]
57. Park, Y.K.; Aghalayam, P.; Vlachos, D.G. A generalized approach for predicting coverage-dependent reaction parameters of complex surface reactions: Application to H<sub>2</sub> oxidation over platinum. *J. Phys. Chem. A* **1999**, *103*, 8101–8107. [[CrossRef](#)]
58. Aloisio, S.; Francisco, J. Existence of a Hydroperoxy and Water (HO<sub>2</sub>-H<sub>2</sub>O) Radical Complex. *J. Phys. Chem. A* **1998**, *102*, 1899–1902. [[CrossRef](#)]
59. Chiorino, A.; Manzoli, M.; Menegazzo, F.; Signoretto, M.; Vindigni, F.; Pinna, F.; Boccuzzi, F. New insight on the nature of catalytically active gold sites: Quantitative CO chemisorption data and analysis of FTIR spectra of adsorbed CO and of isotopic mixtures. *J. Catal.* **2009**, *262*, 169–176. [[CrossRef](#)]

60. Comotti, M.; Li, W.C.; Spliethoff, B.; Schüth, F. Support Effect in High Activity Gold Catalysts for CO. *J. Am. Chem. Soc.* **2006**, *128*, 917–924. [[CrossRef](#)] [[PubMed](#)]
61. Qi, L.; Tang, C.; Zhang, L.; Yao, X.; Cao, Y.; Liu, L.; Gao, F.; Dong, L.; Chen, Y. Influence of cerium modification methods on catalytic performance of Au/mordenite catalysts in CO oxidation. *Appl. Catal. B* **2012**, *127*, 234–245. [[CrossRef](#)]
62. Haneda, M.; Suzuki, K.; Sasaki, M.; Hamada, H.; Ozawa, M. Catalytic performance of bimetallic PtPd/Al<sub>2</sub>O<sub>3</sub> for diesel hydrocarbon oxidation and its implementation by acidic additives. *Appl. Catal. A* **2014**, *475*, 109–115. [[CrossRef](#)]
63. Li, N.; Chen, Q.Y.; Luo, L.F.; Huang, W.X.; Luo, M.F.; Hu, G.S.; Lu, J.Q. Kinetic study and the effect of particle size on low temperature CO oxidation over Pt/TiO<sub>2</sub> catalysts. *Appl. Catal. B* **2013**, *142*, 523–532. [[CrossRef](#)]

**Sample Availability:** Samples of the compounds are available from the authors.



© 2017 by the authors. Licensee MDPI, Basel, Switzerland. This article is an open access article distributed under the terms and conditions of the Creative Commons Attribution (CC BY) license (<http://creativecommons.org/licenses/by/4.0/>).